Available online at www.sciencedirect.com

jmr&t Journal of Materials Research and Technology

journal homepage: www.elsevier.com/locate/jmrt

Original Article

Dynamic modeling and in-process parametric compensation for fabricating micro straight thin walls by micromilling

Yang Li [a], Xiang Cheng [a,*], Guangming Zheng [a], Jiwang Yan [b], Huanbao Liu [a], Xuewei Li [a]

[a] School of Mechanical Engineering, Shandong University of Technology, Zibo, 255000, China
[b] Department of Mechanical Engineering, Keio University, Yokohama, 223-8522, Japan

ARTICLE INFO

Article history:
Received 27 February 2022
Accepted 24 March 2022
Available online 28 March 2022

Keywords:
Micromilling
Thin wall
Elastic deformation
Dimensional error
Dynamic modeling
In-process iterative compensation

ABSTRACT

A comprehensive dynamic model is introduced try to further reduce dimensional errors of micromilled micro straight thin walls based on an in-process cutting parameter compensation device. First, a mathematical model is established to predict the dynamic elastic deformation of the thin walls in the micromilling process. Next, the radial deformation and the runout of the cutter are modeled. Then, the comprehensive in-process parametric compensation model and strategy are established. Finally, a real-time in-process cutting force measurement and cutting parameter compensation device is applied to the micromilling system and thin wall fabrication experiments have been conducted. It shows that the comprehensive dimensional error model and iterative compensation method are effective, and the dimension and shape precision of the micro straight thin wall has been obviously improved after the compensation of the radial cutting depth. The average relative errors have been reduced from 6.86% to 1.10%~1.70%. The in-process compensation method introduced in this study is efficient and convenient as long as compensation strategies are integrated in the controlling unit for a specific micromilling process.

1. Introduction

Micro thin wall parts are widely used in precision instruments, automotive, aeronautical and aerospace industries [1]. In the micromilling process of thin walls, the low rigidity of the parts may cause elastic deformation due to the existence of radial cutting forces. At the same time, the cutter will also undergo radial deformation and runout, which result in the deviation of cutter-part engagement boundaries from the nominal positions and lead to unavoidable surface form errors [2]. Therefore, the prediction and compensation of the elastic deformation of the workpiece and the cutter radial deformation and runout in the milling of micro thin wall parts is of significant importance.

* Corresponding author.
E-mail address: chengxsdut@163.com (X. Cheng).

https://doi.org/10.1016/j.jmrt.2022.03.138

The research of thin wall deformation mainly focuses on three aspects, namely deformation prediction, deformation control and deformation compensation. The off-line Finite Element simulation method is widely adopted for thin wall parts manufacturing. For this method, the force-induced deformation is predicted before machining and then compensated by modifying the original cutter path. Rai et al. built a finite element simulation model of the cutting process by comprehensively considering the factors such as tool, tool path, machining sequence, and cutting parameters, which can realize the prediction of elastic–plastic deformation of integral structural parts [3]. Budak et al. adopted the iterative calculation method to predict cutting force and force-induced deformation during the peripheral milling of thin wall parts in order to solve the coupling problem [4,5]. Based on the prediction of force-induced error, Ratchev et al. proposed an error compensation method for milling low-rigidity thin wall workpieces [6–8]. Wan et al. realized the control of workpiece dimensional error in peripheral milling of thin wall parts based on the proposed mechanical force model and improved FE model [9–11]. Li et al. proposed a structural stiffness modification method for workpiece in-process modeling and finally well predicted the dimensional error of workpiece surface in 5-axis flank milling of thin wall workpieces [12]. Cho et al. checked the machined workpiece using a touch-trigger probe installed on the machine spindle and then made error correction for the same workpiece [13]. Bi et al. proposed an adaptive approach to compensate the deformation error, which obtained by coordinate data obtained with the OMM (on-machine measurement) system [14]. Bi et al. developed an isometric mapping method to compensate the normal deformation by establishing the mapping relationship between the measured real surface and nominal surface [15]. Chen et al. proposed a unified analytical cutting force model for variable helical end milling cutters based on predictive machining theory, which took into account the influence of cutter runout on milling forces [16]. Yue et al. predicted the milling force model based on the chip thickness after the deformation of the workpiece and the contact relationship between the single-edged cutter and the workpiece. The milling force was predicted and an error prediction model was established based on the obtained deformation matrix and force deflection [17]. On this basis, deformation error was compensated by cutter path adjustment [18]. The full compensation process was widely adopted in the existing real-time compensation methods, which effectively compensate the cutting force induced deformation in small cutting depth machining, low-speed machining and small thin wall parts machining [19,20].

Furthermore, even the small error will have a great impact on the experimental results in the process of micromachining, so the accuracy and stability of experimental equipment and measurement equipment should have very high requirements. At the same time, in the process of mathematical modeling more factors than traditional milling need to be considered. Nieslony et al. proposed the problem of precise turning of the mould parts with variable compliance and demonstrated a topographic inspection of the machined surface quality. The stiffness measurement of the machining system and the investigation of cutting force components were studied. The characteristic chatter marks were observed when the turning processes were unstable, and process dynamics had greater contribution in formation of surface finish than turning kinematics and elastic plastic deformation of workpiece [21]. Ranjan proposed an effective method to monitor and detect tool wear and tool breakage by dealing with the vibration signals and cutting force signals that produced by various sensors. Furthermore, this work also developed an adaptive neuro fuzzy inference system (ANFIS) model using different time domains and wavelet packet features of these sensor signals for the prediction of the hole quality. The

Fig. 1 – Influence factors of dimensional errors.

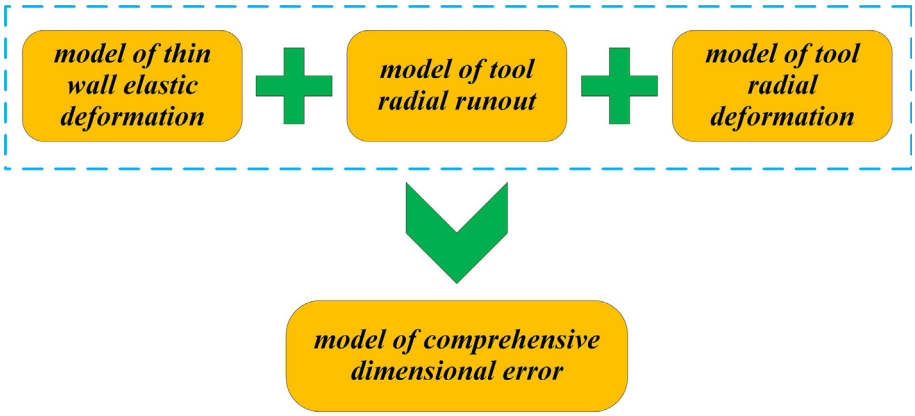

Fig. 2 – Comprehensive dimensional error modelling.

best prediction of hole quality was obtained by a combination of different sensor features in wavelet domain of vibration signal [22]. Wojciechowski proposed a method to predict the cutting force in the micro end milling process with considering the chip thickness accumulation phenomenon. The proposed force model considered the micro end milling kinematics, geometric errors of the machine tool–tool holder-mill system, elastic and plastic deformations of workpiece correlated with the minimum uncut chip thickness, and flexibility of the slender micro end mill. The results showed that the instantaneous and average micromilling forces determined using the proposed model have considerably better conformity with the experimental forces than those predicted by the commonly used rigid micro end milling model [23].

In summary, a series of studies have been carried out on the deformation of micro thin wall parts in milling, and a variety of cutting parameter compensation methods for the deformation of thin wall parts have been put forward to continuously improve the processing quality. However, there are limited studies on micro straight thin wall machining considering the influence of cutter radial deformation error and cutter radial runout error. In this study, in order to further reduce the machining error of micro thin wall produced by thin wall elastic deformation, cutter radial runout and deformation, the comprehensive real-time deformation model is established for both thin walls and cutters, which is used for the in-process compensation of micro thin walls based on a cutting force measurement and parametric compensation device. Micromilling experiments are performed to demonstrate the feasibility of the models, and the micro straight thin walls with good dimensional precision and shape precision are fabricated.

2. Deformation analysis and modeling

2.1. *Deformation analysis for micro straight thins walls*

There are many factors affecting the thin wall fabrication errors, such as workpiece material properties, residual stress, cutting force and cutting heat, process parameters, and clamping condition, etc., as shown in Fig. 1. This study mainly focuses on the thin wall elastic deformations, the cutter deformation and radial runout, as shown in Fig. 2, since these three factors have significant influences on the dimensional accuracy of micro thin walls.

2.2. *Thin wall elastic deformation model*

It is easy to cause elastic deformation of thin walls due to the radial cutting force, resulting in that the actual radial cutting depth is less than the nominal one. Consequently, the finished thin wall will form a large dimensional error. Therefore, it is necessary to accurately measure or predict the thin wall deformation value, and then reduce the dimensional error by compensations.

In this study, the cantilever beam deformation theory is used to analyze and solve the deformation of thin walls. Namely, the elastic deformation process of thin walls subjected to radial cutting force is regarded as the deformation process of cantilever beam. In the actual cutting process, the lower part of the thin wall is fixed by the fixture and the upper part is suspended. Therefore, the thin wall could be simplified into a cantilever beam structure as shown in Fig. 3. The peak cutting force produced in the process is applied to the cantilever beam as a concentrated load of F.

The coordinate system is established as shown in Fig. 3, and the bending moment on any cross section of the cantilever beam can be expressed by Eq. (1).

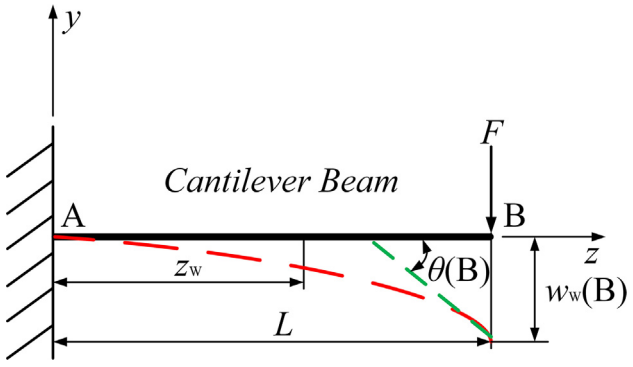

Fig. 3 – Diagram of a thin wall simplified as a cantilever beam.

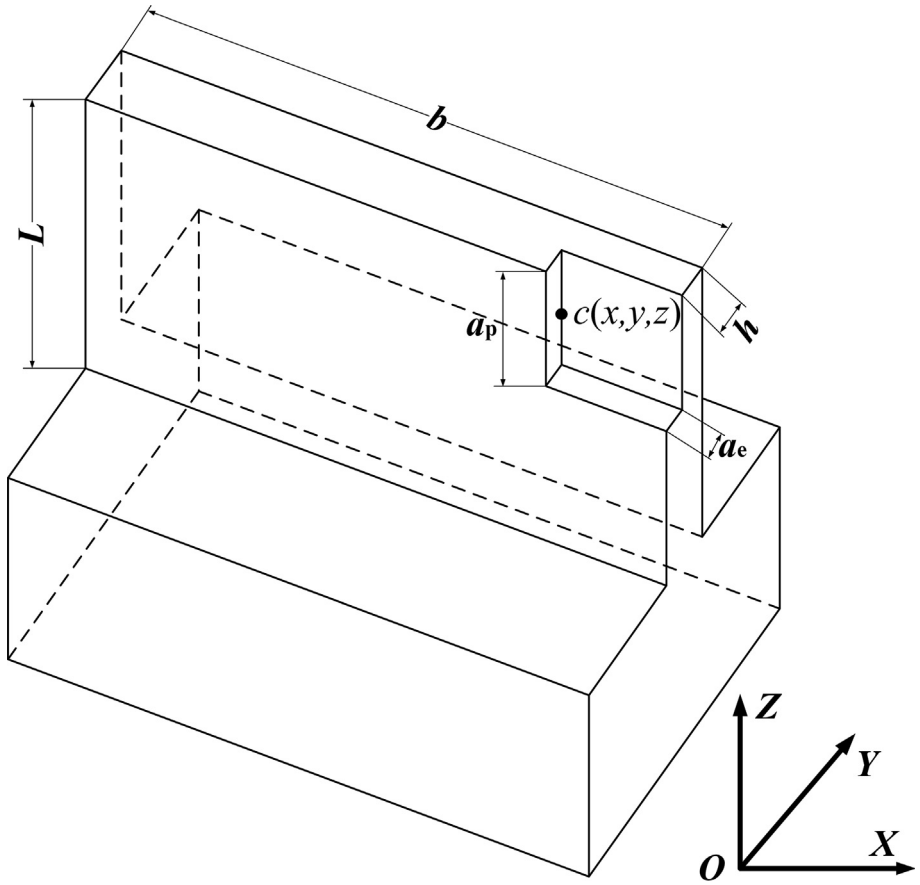

Fig. 4 – Diagram of thin wall shape change in micromilling process.

$$M = -F(L - z_W) \tag{1}$$

where, z_W is a point 2 on the cantilever beam, F is the radial cutting force perpendicular to the direction of the thin wall generated in the process of thin wall machining, L is the length of the cantilever beam, and M is the bending moment at z_W point on the cantilever beam.

The approximately differential equation of cantilever beam deformation is shown in Eq. (2).

$$\frac{d^2 w_W}{dz_W^2} = \frac{M}{E_W I_W} \tag{2}$$

where, w_W is the deformation of the cantilever beam at a certain point, E_W is the elastic modulus of the workpiece material, and I_W is the moment of inertia of the workpiece.

Eq. (3) can be obtained by simplifying Eqs. (1) and (2).

$$E_W I_W w_W'' = M = -F(L - z_W) \tag{3}$$

Eq. (4) can be obtained by integrating Eq. (3) once and twice.

$$\begin{cases} E_W I_W w_W' = \frac{1}{2} F z_W 2 - F L z_W + C \\ E_W I_W w_W = \frac{1}{6} F z_W 3 - \frac{1}{2} F L z_W 2 + C z_W + D \end{cases} \tag{4}$$

where, w_W' is the deflection angle, and C and D are the integration constants.

Since the point A of the cantilever beam is fixed, the values of deflection angle $w_W'(A)$ and deformation $w_W(A)$ at point A are both 0, that is, when $z_W = 0$, Eq. (5) can be obtained.

$$\begin{cases} w_W'(A) = \theta(A) = 0 \\ w_W(A) = 0 \end{cases} \tag{5}$$

Substitute the boundary condition Eq. (5) into Eq (4), and Eq. (6) can be obtained.

$$\begin{cases} C = E_W I_W \theta(A) = 0 \\ D = E_W I_W w_W(A) = 0 \end{cases} \tag{6}$$

Then the integration constants C and D are substituted into Eq. (4), and the equation of deflection angle and deformation equations are obtained as Eq. (7).

$$\begin{cases} E_W I_W w_W' = \frac{1}{2} F z_W^2 - F L z_W \\ E_W I_W w_W = \frac{1}{6} F z_W^3 - \frac{1}{2} F L z_W^2 \end{cases} \tag{7}$$

Eq. (8) can be obtained by simplifying Eq. (7).

$$\begin{cases} w_W' = \left(\frac{1}{2} z_W - L\right) F z_W \Big/ E_W I_W \\ w_W = \left(\frac{1}{6} z_W - \frac{1}{2} L\right) F z_W^2 \Big/ E_W I_W \end{cases} \tag{8}$$

For thin wall parts with the same size and material, the

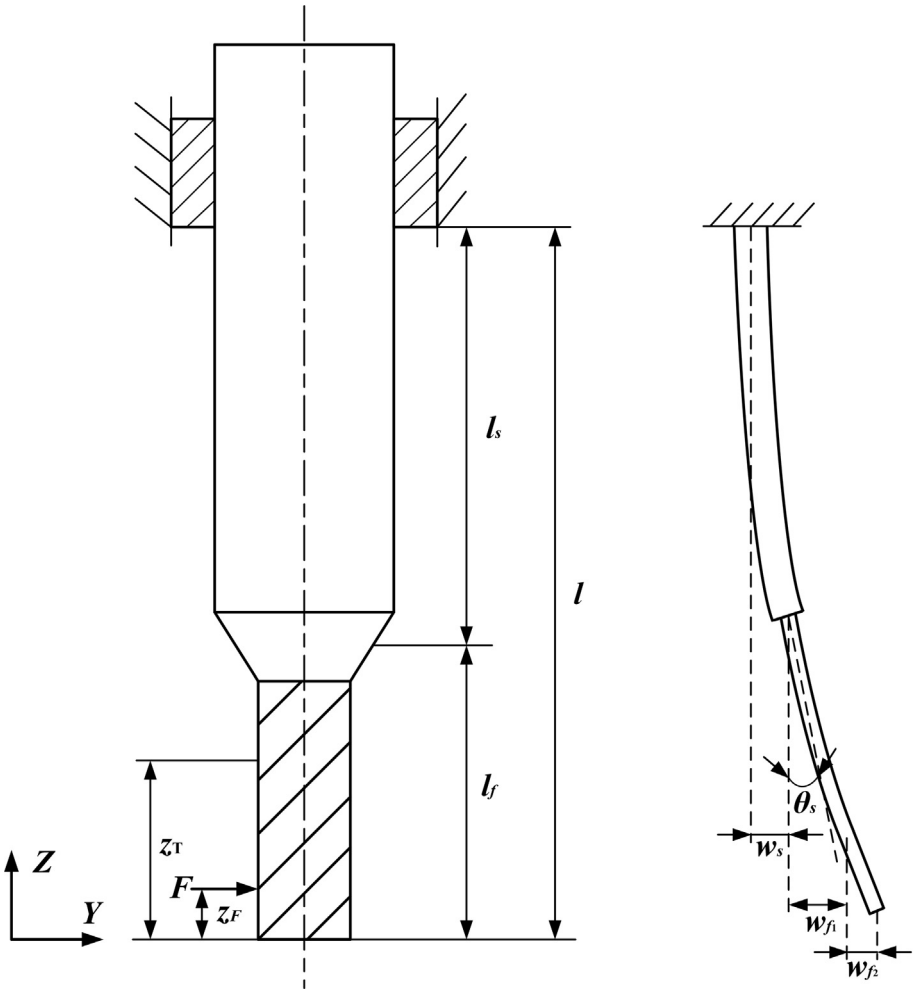

Fig. 5 – Diagram of the radial deformation of the cutter.

length L of the workpiece, the elastic modulus E_W and the moment of inertia I_W of the workpiece are all fixed. According to Eq. (8), it can be concluded that the deformation w_W of a certain position of the thin wall workpiece is only related to the cantilever beam force application position z_W and the cutting force value F for the position.

Since the thin wall material is continuously removed in the actual cutting process as shown in Fig. 4, the moment of inertia is changing dynamically and cannot be regarded as a constant value. A function of the moment of inertia changing with the process of machining needs to be established. Eq. (9) shows the definition of standard rectangular section moment of inertia in material mechanics.

$$I_W = \int_{-h/2}^{h/2} by^2 dy = bh^3/12 \tag{9}$$

Based on the definition of moment of inertia, a coordinate system as shown in Fig. 4 is established. The thin wall can be divided into two parts along the Z-axis direction according to the position of the axial cutting depth. The two parts of moment of inertia can be expressed respectively, and the mean value of the two parts' moment of inertia is taken as the actual one in thin wall cutting process.

The moment of inertia of the two parts along the Z-axis can be expressed in Eq. (10) according to the definition of the moment of inertia in Eq. (9).

$$\begin{cases} I_W(1) = \int_{-h/2+a_e}^{h/2} by^2 dy + \int_{-h/2}^{-h/2+a_e} (x_c + b/2)\, y^2 dy \\ I_W(2) = \int_{-h/2}^{h/2} by^2 dy \end{cases} \tag{10}$$

Eq. (10) is integrated along the Z-axis, and then the average value is taken as the average moment of inertia of the whole thin wall, as shown in Eq. (11).

$$I_W = \left(\int_{z_c - a_p/2}^{l} I_W(1) dz_W + \int_{0}^{z_c - a_p/2} I_W(2) dz_W \right) \Big/ L \tag{11}$$

Therefore, the actual thin wall deformation equation can be expressed by Eq. (12).

$$w_W = \left(\frac{1}{6} z_W - \frac{1}{2} L \right) F z_W^2 / E_W I_W \tag{12}$$

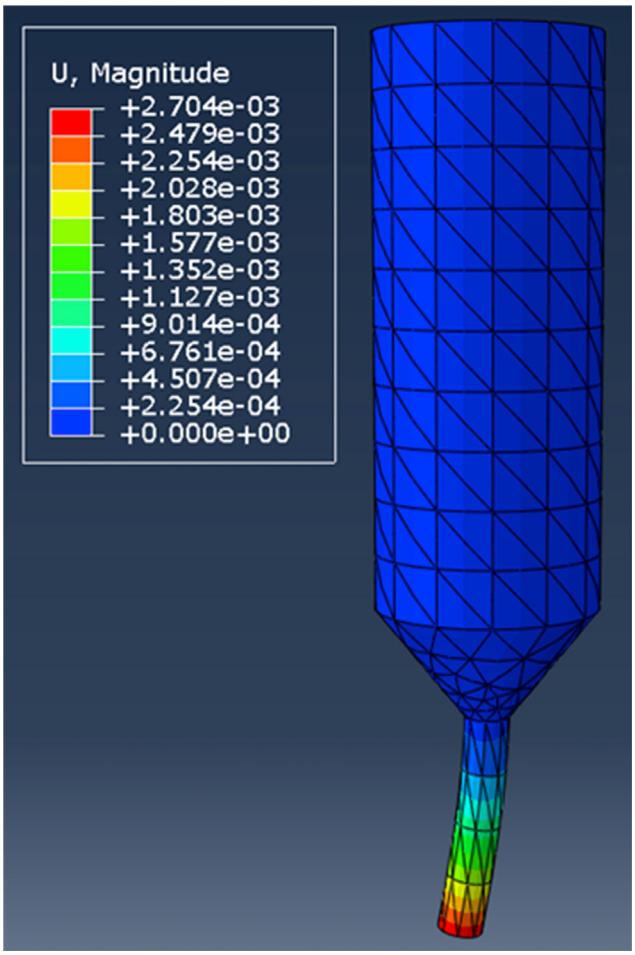

Fig. 6 – Finite element simulation results of tool radial deformation.

2.3. *Cutter radial deformation model*

Even though the stiffness of the cutter is much greater than that of the thin wall workpiece, the radial cutting force generated in the process of thin wall machining will also cause the radial deformation of the cutter. Any dimensional error in micro machining will directly affect the machining quality of the workpiece. Therefore, it is also necessary to accurately measure or predict the cutter deformation, and then compensate the cutter deformation value.

The milling cutter is simplified into a cylindrical cantilever beam model as shown in Fig. 5. The radial deformation of the cutter can be expressed by Eq. (13) [24].

$$w_T = \frac{F}{6E_T I_T}\left[< z_F - z_T >^3 - (l - z_T)^3 + 3(l - z_T)^2(l - z_F)\right] \tag{13}$$

where, the $< >$ is the window function, $< z_F - z_T > = \begin{cases} z_F - z_T, & z_F \geq z_T \\ 0, & z_F < z_T \end{cases}$. F is the radial cutting force perpendicular to the cutter feed direction generated in the thin wall cutting process, w_T is the deformation of the cutter at a certain point, I_T is the moment inertia of the cutter section, E_T is the elastic modulus of the cutter material, l is the cutter length, z_F is the position of the force applied, and z_T is the position of the cutter deformation.

As shown in Fig. 5, the cutter actually consists of two parts, the cutter shank part and the cutting flute part. Therefore, Eq. (13) should be modified according to the geometrical changes of the cutter along the Z-axis. At the same time, because there are chip grooves on the cutter flute part, the moment of inertia of its section cannot be directly expressed by the cutter diameter. It is necessary to approximate the effective diameter of the cutter to simplify the calculation of the moment of inertia, and the diameter of the cutter flute part with the chip groove is usually expressed as 0.8 times the cutter diameter. Therefore, the final cutter deformation can be expressed as Eq. (14).

$$\begin{aligned} w_T &= w_s + w_{f_1} + w_{f_2} \\ &= \frac{F}{6E_T I_s}\left[-(l - l_f)^3 + 3(l - l_f)^2(l - z_F)\right] \\ &+ \frac{F}{6E_T I_f}\left[< z_F - z_T >^3 - (l_f - z_T)^3 + 3(l_f - z_T)^2(l_f - z_F) \right. \\ &\left. \times \right] + (l_f - z_F)\sin\theta_s \end{aligned} \tag{14}$$

$$\theta_s = \frac{F}{2E_T I_s}\left[-(l - l_f)^2 + 2(l - l_f)(l - z_F)\right]$$

where: w_s is the deformation of the cutter shank part, w_f is the deformation of the cutter flute part, θs is the deflection angle of the cutter shank part, l_f is the length of the cutter flute part, I_f is the moment of inertia of the cutter flute part, I_s is the moment of inertia of the cutter shank part.

In order to verify the accuracy of the cutter deformation model, the static simulation experiment of the cutter deformation is carried out as shown in Fig. 6.

A total of nine groups of cutter deformation data can be obtained by applying three different loads to three different positions of the cutter. The nine groups of data are compared with the calculation results of the model to verify the accuracy of the model as shown in Table 1.

According to the results shown in Table 1, it is found that the relative errors between simulation results and calculation results are between 5.2% and 8.3%. The errors are relatively stable and within an acceptable range, indicating that the established mathematical model is reliable and can be used for the prediction of cutter deformations.

Table 1 – Simulation and calculation results of cutter radial deformation.

z_F	F	Simulation result	Calculation result	Relative error
0	0.4	2.70	2.9	6.9%
	0.6	4.06	4.4	7.7%
	0.8	5.41	5.9	8.3%
0.2	0.4	2.56	2.7	5.2%
	0.6	3.83	4.1	6.6%
	0.8	5.11	5.5	7.1%
0.4	0.4	2.36	2.5	5.6%
	0.6	3.53	3.8	7.1%
	0.8	4.72	5.1	7.5%

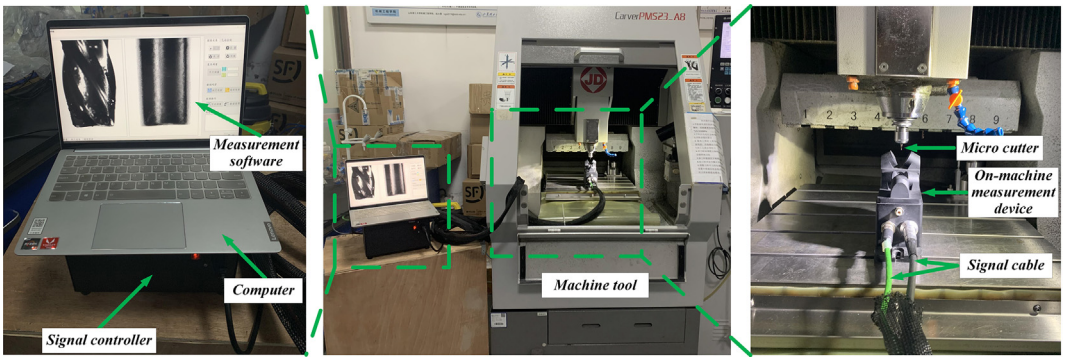

Fig. 7 – Micro cutter measurement system.

2.4. *Cutter radial runout model*

A radial total runout of cutter tip relative to workpiece is created considering the coupling effect of cutter installation error, cutter holder manufacturing error and spindle runout, etc. The radial total runout of cutter tip is in the same order of magnitude as the feed per tooth in the micro-cutting process comparing with the traditional cutting process. Therefore, its influence on the micro-cutting process cannot be ignored. This study will directly conduct quantitative analysis of the radial total runout of cutter tip by relative experiments considering that spindle speed and cutter overhang are the two factors that have the greatest influence on the radial total runout of cutter tip.

Eq. (15) is used to describe the relationship between radial total runout of cutter tip and spindle speed and cutter overhang in the actual cutting process.

$$R = k\, n^{b_1} l^{\,b_2} \tag{15}$$

where, R is the radial total runout of cutter tip, k is the correction coefficient, n is the spindle sped, l is the cutter overhang, b_1 is the influence index of spindle speed on the radial total runout of cutter tip, b_2 is the influence index of cutter overhang on the radial total runout of cutter tip.

Based on Eq. (15), the total runout of cutter tip in radial direction can be calculated at any spindle speed and cutter overhang within the experimental parameter range. In this study, the micro-cutter measurement system is used to measure the radial runout of the cutter tip, as shown in Fig. 7. The coefficient of Eq. (15) is identified by linear regression least squares estimation method, and the prediction model of the total radial runout of the cutter tip is finally expressed.

2.4.1. *Experimental measurement of cutter radial runout*

The experimental factors are cutter overhang and spindle speed, and the experimental index is the radial total runout of cutter tip. Totally five values are selected for each factor, as shown in Table 2.

Table 2 – Experimental parameter selection and measurement results of total runout of cutter tip.

R/μm	12	14	16	18	20
10,000	1.7	1.8	2.1	2.2	2.6
15,000	2.0	2.2	2.3	2.7	2.9
20,000	2.4	2.5	2.7	3.0	3.1
25,000	2.9	3.3	3.4	3.7	3.9
30,000	3.4	3.6	3.8	3.9	4.3

A four-edge end milling cutter with nominal diameter (D) of 1 mm is selected to conduct the radial total runout of cutter tip experiment. The diameter (D_h) of the cutter tip in high-speed rotation is measured, and the radial total runout of cutter tip could be obtained by Eq. (16).

$$R = (D_h - D)/2 \tag{16}$$

2.4.2. *Experimental results and parameter solving*

The experimental results in Table 2 are analyzed to obtain the influence trend of experimental factors on experimental index as shown in Figs. 8 and 9. At the same time, the linear regression least square estimation method is used to identify the parameters in Eq. (15) of the prediction model for radial total runout of the cutter tip, so as to obtain the prediction model for radial total runout of the cutter tip.

Since Eq. (15) is a nonlinear equation, the logarithms commonly used on both sides of Eq. (15) are taken respectively to transform it into a linear Eq. (17).

$$\lg R = \lg k + b_1 \lg n + b_2 \lg l \tag{17}$$

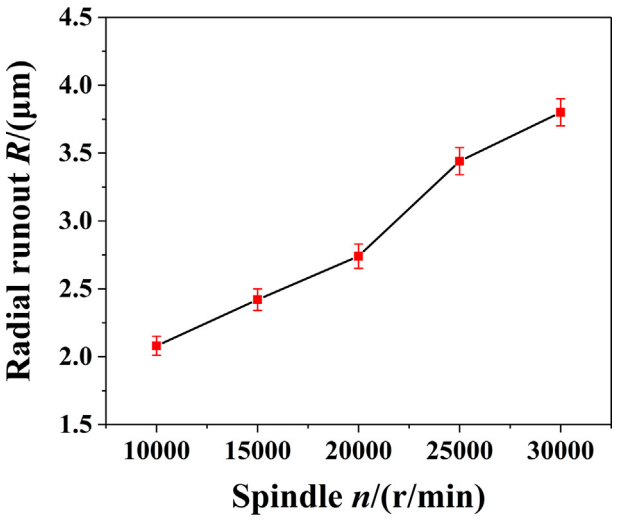

Fig. 8 – The influence of spindle speed on radial total runout of cutter tip.

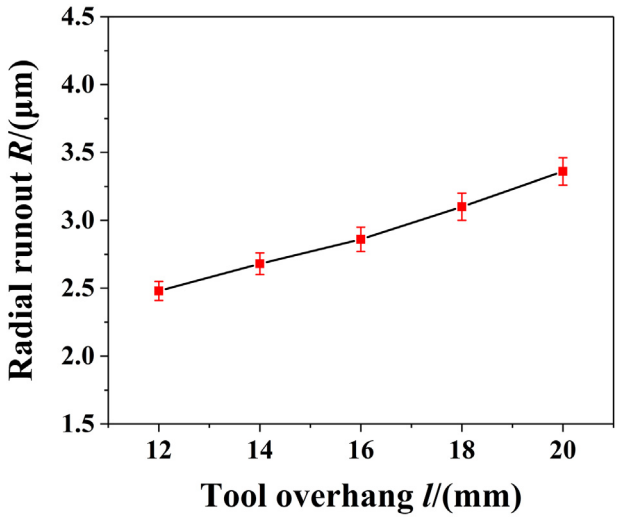

Fig. 9 – The influence of cutter overhang on radial total runout of cutter tip.

Then, make $b_0 = \lg k$, $x_1 = \lg n$, $x_2 = \lg l$, and its corresponding linear regression equation is Eq. (18).

$$y = b_0 + b_1 x_1 + b_2 x_2 \tag{18}$$

The linear equation has a linear relationship between the independent variables x_1, x_2 and the factor y. There are two independent variables x_1 and x_2, and the experimental results are represented by y. A total of 25 groups of experiments have been conducted. The independent variables of the experiment in group i are marked as x_{i1}, x_{i2}, and the experimental results are marked as y_i.

A multiple linear regression Eq. (19) can be established based on the above data due to the existence of experimental error ε.

$$\begin{cases} y_1 = \beta_0 + \beta_1 x_{11} + \beta_2 x_{12} + \varepsilon_1 \\ y_2 = \beta_0 + \beta_1 x_{21} + \beta_2 x_{22} + \varepsilon_2 \\ \cdots\cdots\cdots\cdots\cdots\cdots\cdots \\ y_{24} = \beta_0 + \beta_1 x_{241} + \beta_2 x_{242} + \varepsilon_{24} \\ y_{25} = \beta_0 + \beta_1 x_{251} + \beta_2 x_{252} + \varepsilon_{25} \end{cases} \tag{19}$$

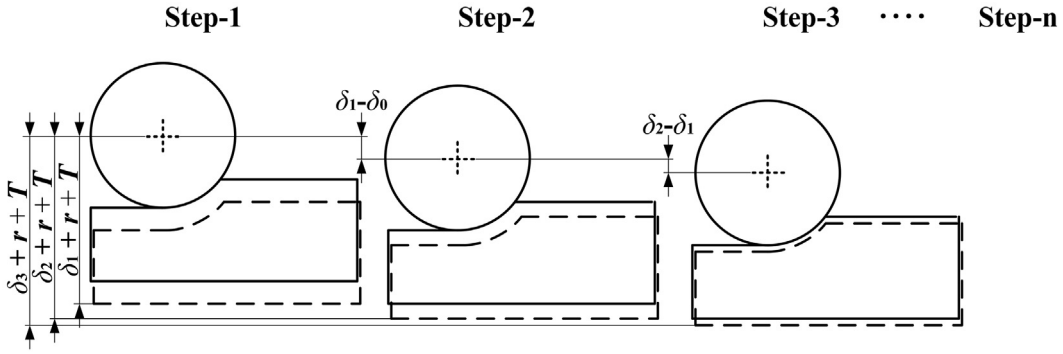

Fig. 10 – The complete compensation strategy of micro thin wall comprehensive dimensional error.

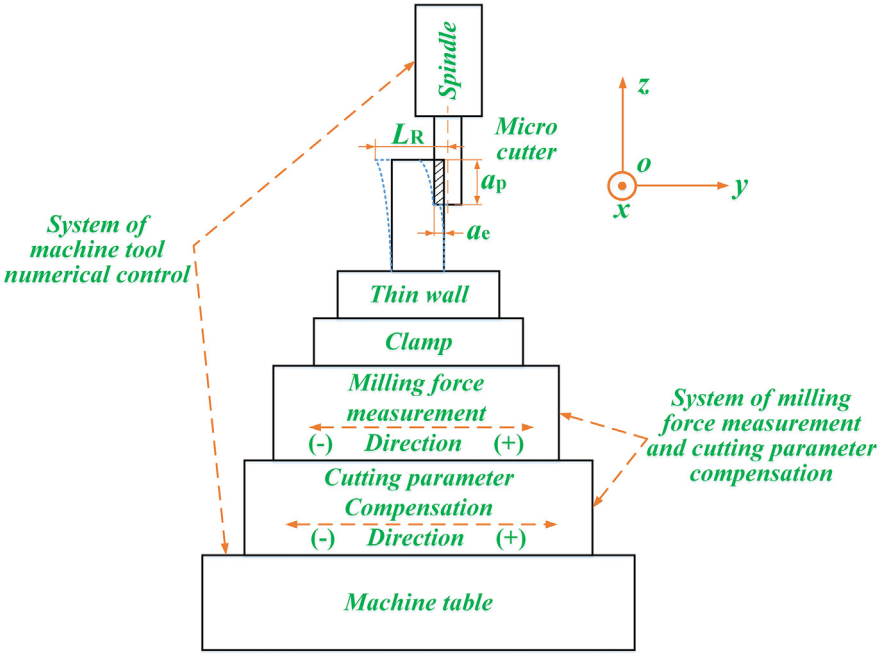

Fig. 11 – Diagram of the dimensional error compensation process.

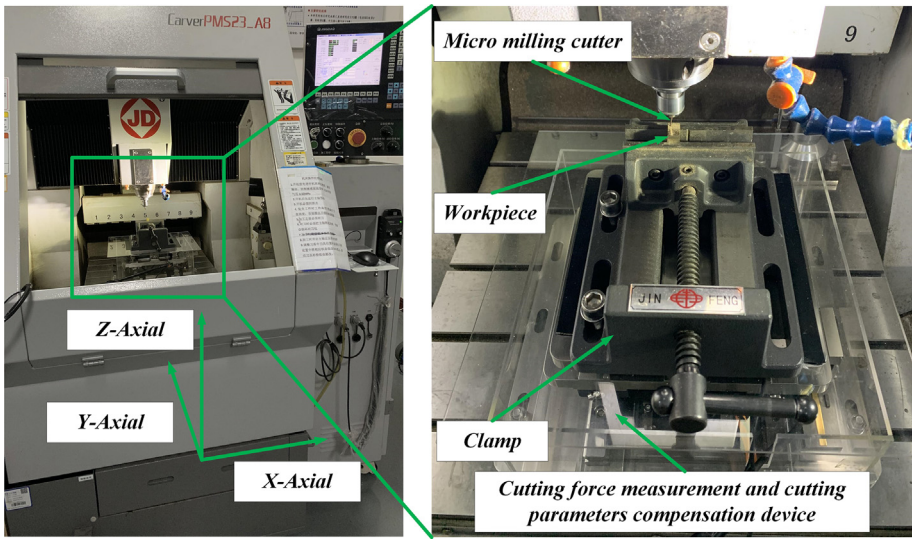

Fig. 12 – Experiment setup.

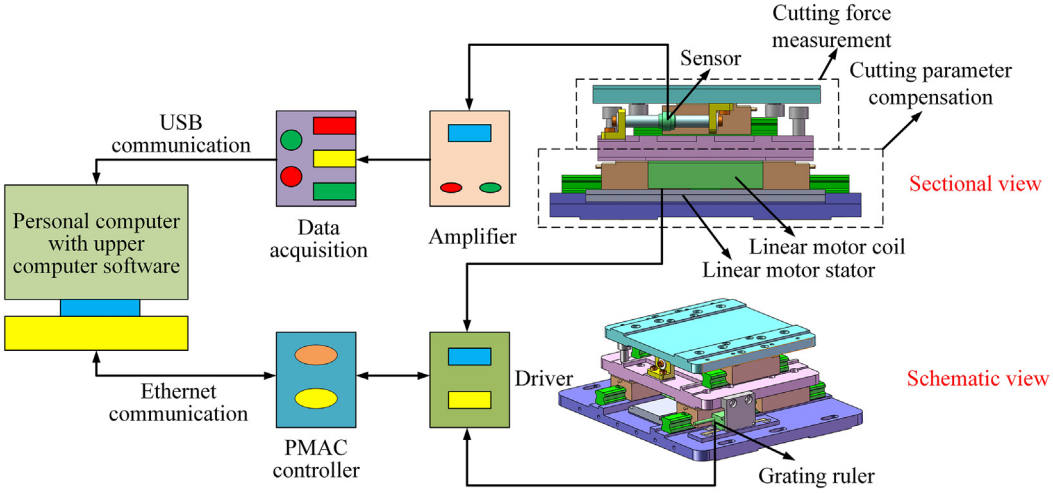

Fig. 13 – The schematic view of the experimental system.

Eq. (19) can be expressed in matrix form of $Y = X\beta + \varepsilon$, so Eq. (20) can be obtained.

$$Y = \begin{pmatrix} y_1 \\ y_2 \\ \vdots \\ y_{24} \\ y_{25} \end{pmatrix} X = \begin{pmatrix} 1 & x_{11} & x_{12} \\ 1 & x_{21} & x_{22} \\ \vdots & \vdots & \vdots \\ 1 & x_{241} & x_{242} \\ 1 & x_{251} & x_{252} \end{pmatrix} \varepsilon = \begin{pmatrix} \varepsilon_1 \\ \varepsilon_2 \\ \vdots \\ \varepsilon_{24} \\ \varepsilon_{25} \end{pmatrix} \beta = \begin{pmatrix} \beta_0 \\ \beta_1 \\ \beta_2 \end{pmatrix} \tag{20}$$

In order to estimate the parameter, the least square method is adopted. Variables b_0, b_1 and b_2 are the least square estimates of the parameters β_0, β_1 and β_2, respectively. Then the regression Eq. (21) can be obtained.

$$\hat{y} = b_0 + b_1 x_1 + b_2 x_2 \tag{21}$$

where, b_0, b_1 and b_2 are regression coefficients.

The value of b can be solved by Eq. (22).

$$b = (X'X)^{-1}X'Y \tag{22}$$

where, X' is transpose matric of X, and $(X'X)^{-1}$ is the inverse matric of $(X'X)$.

The logarithms of the constants in Table 2 are taken respectively to obtain the matrixes X and Y_x, and Eq. (23) can be obtained by substituting matrixes X and Y_x into Eq. (22).

Table 3 – The specifications of the micromilling cutter.

Diameter	Spiral Angle	Cutting Edges	Cutting Edge Radius	Matrix	Coating
1 mm	35°	4	5 μm	Carbide	TiAlN

Table 4 – The specifications of the workpiece material.

Material	Elastic Modulus (N/mm^2)	Shear Elastic Modulus (N/mm^2)	Poisson Ratio	Thermal Conductivity (W/(m·K))	Specific Heat (J/(kg·K))	Density (kg/m^3)
H59 Brass	100,000	37,593	0.33	110	390	8500

Table 5 – The micromilling parameter selection for thin walls.

No.	Thin wall width (μm)	Thin wall height (μm)	a_e (μm)	a_p (μm)	f_z (μm/z)	spindle (r/min)
1	80	800	50	200	1.6	20,000
2	100					
3	120					

$$b = \begin{cases} -2.7114 \\ 0.5673 \\ 0.6157 \end{cases} \quad (23)$$

Therefore, the prediction model Eq. (24) of the radial total rundout of cutter tip is obtained.

$$R = 0.0019\, n^{0.5673}\, l^{0.6157} \quad (24)$$

Based on Eq. (24), the radial total runout of cutter tip can be quantified under certain process conditions, which is conducive to further analysis of thin wall dimensional error.

2.5. *Comprehensive modelling of micro straight thin walls*

Based on the above established models, the three main factors causing dimensional error of thin wall machining are comprehensively analyzed. The thin wall comprehensive dimensional error model is accurately established, as shown in Eq. (25).

$$w_{Total} = w_T + w_W + R_T \quad (25)$$

where, w_{Total} is the comprehensive dimensional error of the micro thin wall, w_W is the elastic deformation of the micro thin wall, as shown in Eq. (12), w_T is the cutter radial deformation, as shown in Eq. (14), R_T is the cutter radial runout, as shown in Eq. (24).

3. In-process iterative compensation of micro thin wall

In the processing of thin wall parts, the radial cutting depth a_e in the processing program can be expressed as Eq. (26).

$$a_e = T_{initial} - T \quad (26)$$

where, T is the target wall thickness of thin wall parts, and $T_{initial}$ is the initial wall thickness.

The radial cutting depth a_e in machining program is usually expressed by parameter a. However, the thin wall workpiece will produce elastic deformation of $w_W(a)$ and the cutter will produce radial deformation of $w_T(a)$ due to the existence of cutting force generated in micromachining. At the same time, the cutter radial runout R_T also exists in the machining process, resulting in the micro thin wall comprehensive dimensional error $\delta(a)$, as shown in Eq. (27).

$$\delta(a) = w_W(a) + w_T(a) - R_T \quad (27)$$

According to Eq. (27), the existence of dimensional error makes the actual radial cutting depth change to $a-\delta(a)$, which deviates from the nominal radial cutting depth, resulting in machining errors. In order to compensate the dimensional error, it is necessary to adjust the radial cutting depth in the program until the actual radial cutting depth is equal to the required radial cutting depth, that is, Eq. (28) should be satisfied.

$$a = a_e + \delta(a) \quad (28)$$

In Eq. (28), since the dimensional error $\delta(a)$ is a nonlinear function of a, it is difficult to obtain the solution directly through general calculation. Numerical iteration is usually used to solve Eq. (28), and the simplest iteration method is the complete compensation method as shown in Fig. 10.

As shown in Fig. 10, theoretically, the distance L_T from the cutter geometric center to the side of the thin wall feature should be the sum of cutter radius r plus and target thickness T of the thin wall, as shown in Eq. (29).

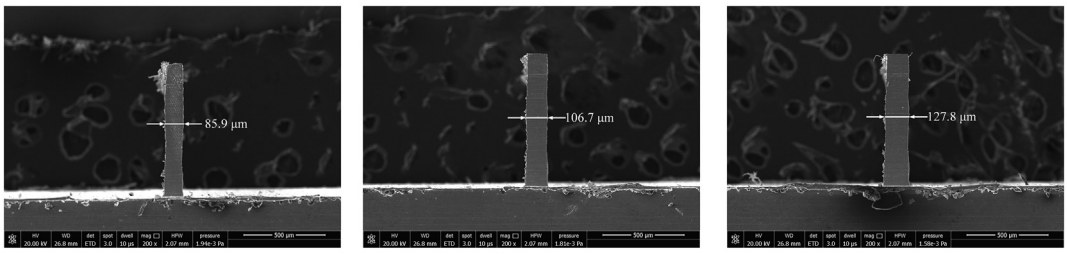

(a) T = 80 μm (b) T = 100 μm (c) T = 120 μm

Fig. 14 – The results of without comprehensive dimensional error compensation (Group 1).

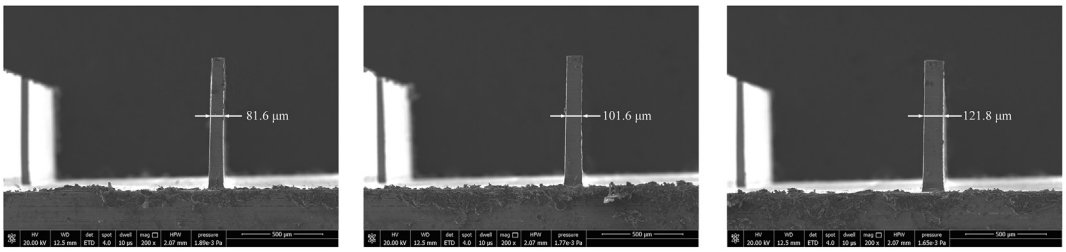

(a) T = 80 μm (b) T = 100 μm (c) T = 120 μm

Fig. 15 – The results of with comprehensive dimensional error compensation (Group 2).

$$L_T = r + T \tag{29}$$

However, this distance is changed due to the elastic deformation of the thin wall, the cutter radial deformation, and the cutter radial runout. The actual distance L_R could be expressed as Eq. (30).

$$L_R = r + T + w_W(a) + w_T(a) - R_T \tag{30}$$

Substituting Eq. (27) into Eq. (30), then Eq. (31) can be obtained.

$$L_R = r + T + \delta(a) \tag{31}$$

Due to the influence of the cutter radial deformation and runout, the geometric center of the cutter changes with the machining process. Therefore, the difference between the actual distance L_R and the theoretical distance L_T can be expressed as Eq. (32).

$$\Delta L = L_R - L_T = \delta(a) \tag{32}$$

As shown in Eq. (32), the value of cutter radius R and thin wall target thickness T are constants. The difference between the actual distance from the cutter geometric center to the side of thin wall feature away from the cutter and the theoretical distance is the comprehensive dimensional error δ(a). According to the definition of complete compensation method, the compensation value is equal to the comprehensive dimensional error value.

Therefore, in Step-1, the comprehensive size error δ_1 can be calculated by Eq. (27) firstly. In Step-2, the deformation distance of the thin wall relative to the cutter geometric center is equal to δ_1, and a new comprehensive dimensional error value δ_2 is generated in Step-2. In Step-3, the deformation distance of the thin wall relative to the cutter geometric center is equal to δ_2–δ_1, and a new comprehensive dimensional error value δ_3 is generated in Step-3. The iterative compensation process continues until machining tolerances are satisfied. In accordance with the principle of complete compensation, the iterative compensation process of radial cutting depth a_{i+1} in the program is shown in Eq. (33).

$$a_{i+1} = a_e + \delta(a_i) \tag{33}$$

The initial value a_1 of a_{i+1} is equal to the radial cutting depth a_e. As shown in Fig. 11, $\delta(a_i)$ is calculated by the equation of thin wall comprehensive dimensional error in real time during the micromilling processing compensation.

The basic principle of iterative compensation for radial cutting depth a_e is to find the root of Eq. (28). Based on Eq. (33), the value of radial cutting depth in the program of the (i+1) iteration of the actual radial cutting depth a_{i+1} is the nominal radial depth a_e with the comprehensive error $\delta(a_i)$ of thin wall machining. Therefore, the iterative function $\Phi(a_i)$ is used to represent the compensation process, as shown in Eq. (34).

$$\Phi(a_i) = a_{i+1} \tag{34}$$

According to the convergence criterion, $\Phi(a_i)$ needs to be updated iteratively until it's equal to a^*.

Eq. (35) can be obtained by constructing the first-order Taylor series approximation of $\Phi(a_i)$ at $a = a^*$.

$$\Phi(a_i) = \Phi(a^*) + \Phi'(a^*)(a_i - a^*) \tag{35}$$

According to Eq. (35) and the conclusion of literature [25], the machining error is converges, but the convergence rate is only in one order. Therefore, the process of iterative compensation for radial cutting depth with the traditional

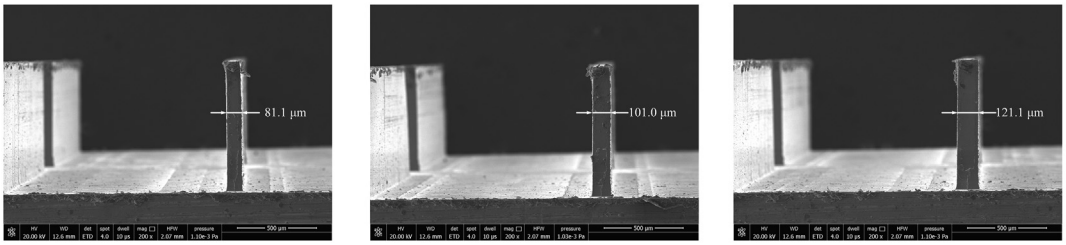

(a) T = 80 μm (b) T = 100 μm (c) T = 120 μm

Fig. 16 – The results of with comprehensive dimensional error iterative compensation (Group 3).

complete compensation method has a slow convergence speed. The compensation problem of radial cutting depth is actually a problem of finding the root of equation. In order to obtain faster convergence speed, a secant algorithm is proposed and introduced into the real-time compensation process. Therefore, the root of Eq. (28) is equivalent to the solution of Eq. (36).

$$F(a) = a - a_e - \delta(a) = 0 \tag{36}$$

The secant algorithm is used to solve the root of Eq. (36) iteratively, and it is found that the value a_{i+1} of the actual radial cutting depth a_e needed to be adjusted iteratively according to Eq. (37) [25].

$$a_{i+1} = a_i - \frac{a_i - a_{i-1}}{F(a_i) - F(a_{i-1})} F(a_i) \tag{37}$$

where, a_{i+1} is the value of the next actual radial cutting depth a_e in the iterative compensation process.

Eq. (38) can be obtained by substituting Eq. (36) into Eq. (37).

$$a_{i+1} = a_i - \frac{a_i - a_{i-1}}{a_i - a_{i-1} - \delta(a_i) + \delta(a_{i-1})}(a_i - a_e - \delta(a_i)) \tag{38}$$

In the actual machining process, the actual radial cutting depth a_e is adjusted by changing the offset between the thin wall and the cutter tip. The offset value Δ_i of the current compensation process can be determined as Eq. (39).

$$\Delta_i = a_{i+1} - a_i = \frac{a_i - a_{i-1}}{a_i - a_{i-1} - \delta(a_i) + \delta(a_{i-1})}(a_e - a_i + \delta(a_i)) \tag{39}$$

According to the convergence analysis of secant algorithm, the convergence speed of the above compensation process is at least 1.618, while the convergence speed of the conventional complete compensation process is only 1 [25]. Therefore, the compensation process can reduce the calculation time and improve the efficiency of the whole compensation process.

4. Micro thin wall fabrication experiment

In order to verify the introduced model and the iterative algorithm, the compensation experiments are conducted respectively. Meanwhile, the conventional micro thin wall milling experiment without comprehensive dimensional error compensation is also conducted as a contrast.

4.1. *Experiment setup*

The CNC milling machine cutter CarverPMS23_A8 is used to conduct the experiments, as shown in Fig. 12. The programming resolution for each linear axis is 0.1 μm. The maximum rotation speed of spindle is 36, 000 min^{-1}.

In order to measure the cutting force produced in thin wall milling process and compensate the radial cutting parameter, a device for cutting force measurement and cutting parameter compensation is developed. Fig. 13 shows the three-dimensional structure and the control system diagram of the designed cutting force measurement and cutting parameter compensation device. It is mainly composed of two components, the cutting force measurement component and the cutting parameter compensation component. The cutting force measurement component is composed of a piezoelectric sensor, two guide rails and slides. The resolution of the piezoelectric sensor is 0.001 N and the comprehensive accuracy is 0.005 N. The cutting parameter compensation component is composed of a linear motor, two guide rails and slides, and a grating ruler. The resolution of the motion system is 0.1 μm and the positioning accuracy is within 0.5 μm. The force signal is amplified and transmitted to the computer after A/D conversion from the USB port and processed by the upper computer to get the final measured cutting force value. The upper computer sends the motion instruction to the PMAC controller through the Ethernet port. The linear motor is used to realize the desired compensation movement.

The working principle of the proposed device is shown in Fig. 11. The spindle is fed in the *X*-direction, and the cutting force measurement system is used to measure the radial cutting force perpendicular to the micro straight thin wall. After reading and processing the cutting force, the upper computer outputs the command to PMAC controller. The device can realize the linear motion perpendicular to the thin wall direction, so as to realize the compensation of the radial cutting parameter. The cutting force measurement and cutting parameter compensation device is fixed on the worktable of the machine. The workpiece is fixed on the proposed device through the clamp.

The specifications of cutter and workpiece used in the experiment are shown in Table 3 and Table 4, respectively. The micromilling parameter selection for thin walls is shown in Table 5 [26,27].

4.2. *Experiment results*

The actual thicknesses of thin walls are measured by scanning electron microscope (Model: Quanta 250) after micromilling. All measurements are averaged by measuring at least six positions. Fig. 14 shows the thin wall thickness measurement results without comprehensive dimensional error compensation. Fig. 15 shows the thin wall thickness measurement results with comprehensive dimensional error compensation. Fig. 16 shows the thin wall thickness measurement results with comprehensive dimensional error iterative compensation.

4.3. *Comparative analysis of the experimental results*

It can be seen from Fig. 14 that the thickness of the thin wall is nonuniform, and has a large dimensional error. Thin wall part produces elastic deformations in the micromilling process due to the large milling force, resulting in the actual radial cutting parameter is less than the nominal radial cutting parameter. Consequently, the thin wall thickness after machining is greater than the nominal thickness.

Fig. 15 and Fig. 16 show that the thickness of the thin wall after in-process compensation is relatively uniform compared that without compensations. The experimental results show that the dimensional errors of the thin walls have been significantly reduced. The average relative errors have been reduced from 6.86% to 1.70% and 1.10% as shown in Table 6. The machining quality has a relatively obvious improvement in dimensional accuracy after the comprehensive dimensional error compensation.

Table 6 – Relative dimensional errors of thin wall.

Group	Nominal thin wall thickness (μm)	Thin wall thickness without error compensation (μm)	Relative error	Thin wall thickness with error compensation (μm)	Relative error	Thin wall thickness with error iterative compensation (μm)	Relative error
1	80	85.9	7.38%	81.6	2.00%	81.1	1.38%
2	100	106.7	6.70%	101.6	1.60%	101.0	1.00%
3	120	127.8	6.50%	121.8	1.50%	121.1	0.92%
Average	100	107.2	6.86%	101.7	1.70%	101.1	1.10%

Table 7 – Shape accuracy of thin wall.

Group	Thin wall thickness (μm)		
	80	100	120
1	Not good	Not good	Not good
2	Average	Good	Good
3	Average	Good	Good

Meanwhile, the thin wall shape accuracy is evaluated. The evaluation criteria for shape accuracy are that the thin wall has not bending deformation and the thin wall thickness is uniform. The evaluation results are shown in Table 7.

The experimental results show that the comprehensive dynamic modeling and in-process parametric compensation method are effective and can be used to compensate the dimensional error of thin wall machining. In theory, the relative errors of thin wall can be reduced to 0.5%. Due to the limitations of the precision of the machine tool, the response frequency of the compensation device, as well as the measurement error of the cutting force and other influences, the relative errors of the thin wall can be reduced to 1.10%.

The proposed method is more convenient than modifying machining procedures for cutting parameter compensations. Thin wall parts with higher precision can be machined on machine tools with relatively lower precision by using the introduced real-time in-process cutting force measurement and cutting parameter compensation device.

5. Conclusions

Considering the dynamic elastic deformation of thin walls, the radial deformation and run out of the micro end mill, the comprehensive in-process parametric compensation model and strategy are established for micro straight thin wall micromilling processes. Comparative experiments show that the dimensional errors of the thin wall are significantly reduced after the in-process radial cutting depth compensations. The average relative errors have been reduced from 6.86% to 1.10%~1.70%. The dimension accuracy of the thin wall has been greatly improved and the shape accuracy of the thin wall has been guaranteed compared with that without compensations. Experimental results show that the established models are reliable, which can be used to compensate the radial cutting depth in micro straight thin wall fabrications in process. The study has some enlightenment in potential applications other than one-dimensional straight thin wall compensations, where two or three dimensional compensation strategies and devices are needed.

Declaration of Competing Interest

The authors declare that they have no known competing financial interests or personal relationships that could have appeared to influence the work reported in this paper.

Acknowledgment

The paper is financially supported by the Natural Science Foundation of Shandong Province (ZR2020ME157), and the National Key Research and Development Program of China (2018YFB2001400).

REFERENCES

[1] Wang F, Cheng X, Zheng GM, Yang XH, Guo QJ, Sun QL. Study of micromilling parameters and processes for thin wall fabrications. Precis Eng 2019;56:246–54.
[2] Wang F, Cheng X, Guo QJ, Yang XH, Zheng GM. Experimental study on micromilling of thin walls. J Micromech Microeng 2018;29:015009.
[3] Rai JK. Finite element method based machining simulation environment for analyzing part errors induced during milling of thin-walled components. Int J Mach Tool Manufact 2008;6:629–43.
[4] Budak E, Altintas Y. Modeling and avoidance of static form errors in peripheral milling of plates. Int J Mach Tool Manufact 1995;35:459–76.
[5] Tsai JS, Liao CL. Finite-element modeling of static surface errors in the peripheral milling of thin-walled workpieces. J Mater Process Technol 1999;94:235–46.
[6] Ratchev S, Liu S, Becker AA. Error compensation strategy in milling flexible thin-wall parts. J Mater Process Technol 2005;162:673–81.
[7] Ratchev S, Liu S, Huang W, Becker AA. Milling error prediction and compensation in machining of low-rigidity parts. Int J Mach Tool Manufact 2004;44:1629–41.
[8] Ratchev S, Liu S, Huang W, Becker AA. An advanced FEA based force induced error compensation strategy in milling. Int J Mach Tool Manufact 2006;46:542–51.
[9] Wan M, Zhang WH, Qin GH, Wang ZP. Strategies for error prediction and error control in peripheral milling of thin-walled workpiece. Int J Mach Tool Manufact 2008;48:1366–74.
[10] Wan M, Zhang WH. Efficient algorithms for calculations of static form errors in peripheral milling. J Mater Process Technol 2006;171:156–65.

[11] Chen W, Xue J, Tang D, Chen H, Qu S. Deformation prediction and error compensation in multilayer milling processes for thin-walled parts. Int J Mach Tool Manufact 2009;49:859–64.
[12] Li ZL, Tuysuz O, Zhu LM, Altintas Y. Surface form error prediction in five-axis flank milling of thin-walled parts. Int J Mach Tool Manufact 2018;128:21–32.
[13] Cho MW, Kim GH, Seo TI, Hong YC, Cheng HH. Integrated machining error compensation method using OMM data and modified PNN algorithm. Int J Mach Tool Manufact 2006;46:1417–27.
[14] Huang N, Bi Q, Wang Y, Sun C. 5-Axis adaptive flank milling of flexible thin-walled parts based on the on-machine measurement. Int J Mach Tool Manufact 2014;84:1–8.
[15] Bi Q, Huang N, Zhang S, Shuai C, Wang Y. Adaptive machining for curved contour on deformed large skin based on on-machine measurement and isometric mapping. Int J Mach Tool Manufact 2019;136:34–44.
[16] Chen D, Zhang X, Xie YK, M Zhang X, Ding H. A unified analytical cutting force model for variable helix end mills. Int J Adv Manuf Technol 2017;92:3167–85.
[17] Yue C, Chen Z, Liang SY, Gao HN, Liu XL. Modeling machining errors for thin-walled parts according to chip thickness. Int J Adv Manuf Technol 2019;103:91–100.
[18] Li ZL, Zhu LM. Compensation of deformation errors in five-axis flank milling of thin-walled parts via cutter path optimization. Precis Eng 2019;55:77–87.
[19] Liu C, Li Y, Shen W. A real time machining error compensation method based on dynamic features for cutting force induced elastic deformation in flank milling. Mach Sci Technol 2018;22:1–21.
[20] Diez E, Perez H, Marquez J, Vizan A. Feasibility study of in-process compensation of deformations in flexible milling. Int J Mach Tool Manufact 2015;94:1–14.
[21] Nieslony P, Krolczyk GM, Wojciechowski S. Surface quality and topographic inspection of variable compliance part after precise turning. Appl Surf Sci 2018;434:91–101.
[22] Ranjan J, Patra K, Szalay T. Artificial intelligence-based hole quality prediction in micro-drilling using multiple sensors. Sensors 2020;20:885.
[23] Wojciechowski S, Matuszak M, Powałka B. Prediction of cutting forces during micro end milling considering chip thickness accumulation. Int J Mach Tool Manufact 2019;147:103466.
[24] Kline WA, DeVor RE, Shareef IA. The prediction of surface accuracy in end milling. ASME J Manuf Sci Eng 1982;104:272–8.
[25] Wang XZ, Li ZL, Bi QZ, Zhu LM, Ding H. An accelerated convergence approach for real-time deformation compensation in large thin-walled parts machining. Int J Mach Cutter Manuf 2019;142:98–106.
[26] Li Y, Cheng X, Ling SY, Zheng GM. On-line compensation for micromilling of high-aspect-ratio straight thin walls. Micromachines 2021;12:603.
[27] Li Y, Cheng X, Ling SY, Zheng GM, He L. Study on deformation and compensation for micromilled thin walls with high aspect ratios. Int J Adv Manuf Technol 2021;117:1797–806.